MATERIALS SCIENCE

Molecularly selective nanoporous membrane-based wearable organic electrochemical device for noninvasive cortisol sensing

Onur Parlak[1]*, Scott Tom Keene[1], Andrew Marais[1], Vincenzo F. Curto[2], Alberto Salleo[1]*

Wearable biosensors have emerged as an alternative evolutionary development in the field of healthcare technology due to their potential to change conventional medical diagnostics and health monitoring. However, a number of critical technological challenges including selectivity, stability of (bio)recognition, efficient sample handling, invasiveness, and mechanical compliance to increase user comfort must still be overcome to successfully bring devices closer to commercial applications. We introduce the integration of an electrochemical transistor and a tailor-made synthetic and biomimetic polymeric membrane, which acts as a molecular memory layer facilitating the stable and selective molecular recognition of the human stress hormone cortisol. The sensor and a laser-patterned microcapillary channel array are integrated in a wearable sweat diagnostics platform, providing accurate sweat acquisition and precise sample delivery to the sensor interface. The integrated devices were successfully used with both ex situ methods using skin-like microfluidics and on human subjects with on-body real-sample analysis using a wearable sensor assembly.

INTRODUCTION

Wearable health monitoring technologies and devices are of great and continuous interest in clinical healthcare due to their ability to monitor physiological signals and to help maintain an optimal health status as well as assess the physical fitness of outpatients (*1*, *2*). In particular, wearable biosensors aim to replace centralized hospital-based care systems with home-based personal diagnostics to reduce healthcare costs and time to diagnosis by providing noninvasive, real-time analysis (*3*, *4*) .Therefore, a wide variety of approaches have been proposed to bring such analysis methodologies closer to patients in both time and space (*5*, *6*). Early research activities on continuous health monitoring using wearable sensors focused on physical sensing (*7*–*9*). These efforts have resulted predominantly in temperature, pressure, and electric field sensors for monitoring biophysical signals including heart rate (*6*), respiration rate (*10*), skin temperature (*11*), and brain activity (*12*). Recent interest, however, focuses on chemical and biochemical sensing to monitor clinically relevant biomarkers using wearable devices to broaden the range of measurable quantities (*13*, *14*). Among many bodily fluids, sweat provides a significant amount of information about a patient's health status and is readily accessible, making it suitable for wearable, noninvasive biosensing (*15*). Sweat contains important electrolytes, metabolites, amino acids, proteins, and hormones, which allows monitoring of metabolic diseases, physiological conditions, or a person's intoxication level (*16*, *17*).

Stress plays an important role in the overall health of a patient; when under stress, the adrenal gland releases cortisol and adrenaline into the bloodstream. The cortisol levels in various bodily fluids can range from 4 pM to 70 μM depending on the fluid. In sweat, the optimum level of cortisol ranges from 0.02 to 0.5 μM (*18*, *19*). Increased levels of cortisol have a detrimental effect on the regulation of various physiological processes such as blood pressure, glucose levels, and carbohydrate metabolism, and sustained stress can disrupt homeostasis in the cardiovascular, immune, renal, skeletal, and endocrine systems, leading to development of chronic diseases (*19*). Therefore, continuous monitoring of cortisol levels in bodily fluids has great relevance in maintaining healthy physiological conditions. As a result, there is much interest in devising wearable devices able to monitor stress levels. Most stress sensors described in the literature are based on physical sensing and mainly focus on monitoring skin perspiration or conductivity, heart rate, and temperature (*6*, *20*). These approaches are promising in terms of fabrication using novel functional materials having desirable mechanical properties such as stretchability, flexibility, and high durability. However, the alteration of bodily physical parameters can also be induced by nonstress-related causes such as weather conditions and fever, making these sensors generally vulnerable to false positives. Furthermore, recent devices often show poor performance in terms of invasiveness, stability of recognition, selectivity, and sample acquisition (*19*). However, in one recent study, Jang *et al.* demonstrated a field-effect transistor-based cortisol sensor by embedding a cortisol antibody into the synthetic polymer matrix to generate a cortisol-selective/sensitive membrane. The designed sensor shows high sensitivity and a low limit of detection (down to 1 pg/ml) (*18*). Here, we describe the development of a wearable biosensor using an organic electrochemical device for the detection of stress by selectively sensing cortisol in sweat.

Recently, electrochemical transducing elements have been developed to directly detect biomarkers from patients (*3*, *21*, *22*). Among electrochemical transducing elements, organic electrochemical transistors (OECTs) are preferred in the field of bioelectronics due to their exceptional ability to interface electronics with biology (*23*, *24*). An OECT consists of a semiconductor polymer channel, typically poly(ethylenedioxythiophene):poly(styrenesulfonate) (PEDOT:PSS), that can be gated through an electrolyte solution (*25*). The ions in solution are pushed by the gate potential to dope/de-dope the entire volume in the organic semiconductor channel, thereby strongly modulating its conductivity (*26*). Hence, OECTs are able to transduce biological

[1]Department of Materials Science and Engineering, Stanford University, 450 Serra Mall, Stanford, CA 94305, USA. [2]Department of Bioelectronics, Ecole Nationale Supérieure des Mines, Centre Microélectronique de Provence–École nationale supérieure des mines de Saint-Étienne, Center Microelectronics De Provence Georges Charpak, 880 Avenue de Mimet, Gardanne 13541, France.
*Corresponding author. Email: parlak@stanford.edu (O.P.); asalleo@stanford.edu (A.S.)

ion-based signals into electrical signals with high gain at relatively low voltages (<0.5 V) (*27*). They have been widely proposed for many applications including water and food safety and health monitoring through detection of biologically relevant ions (*28*), metabolites (*22*), and pathogens (*29*), which are commonly used for diagnostics (*30*). Because cortisol is not charged at physiological pH, OECTs are, in principle, not suitable for its detection. To obviate this drawback and target specific molecules, common biocomponents such as antibodies or enzymes have been used as the specific recognition elements in the fabrication of OECT-based biosensors (*31*). However, these sensors have inherent limitations such as vulnerability to interference from other ions present in the sample solutions and lack of selectivity to a particular analyte even if high-affinity biomolecules are used. Given the often poor chemical and physical stability of these biomolecules, which is especially problematic in wearable devices, artificial receptors have been gaining in importance as a possible alternative to natural systems (*32*). Artificial receptors, such as molecularly imprinted polymers (MIPs), are increasingly becoming recognized as a versatile tool, particularly for the preparation of synthetic polymers containing tailor-made recognition sites (*33*). Hence, to overcome the existing limitations of unstable biorecognition, we developed an MIP-based artificial recognition membrane that is interposed between the PEDOT:PSS channel layer and the analyte (sweat) reservoir to control and regulate the selective molecular transport of cortisol directly from the skin to the OECT sensing channel (Fig. 1A). Here, we report the development of new skin-mounted patch-type molecularly selective OECT (MS-OECT) as a cortisol biosensor by implementing a multifunctional layered device, which can be adapted to other types of sweat-based wearable sensors.

RESULTS

Sensor design and material strategy

The MS-OECT comprises a multifunctional layered structure that achieves selective sensing of cortisol from human sweat (Scheme 1). Briefly, the device consists of a PEDOT:PSS OECT with a planar Ag/AgCl gate as an electrochemical transducing layer functionalized with molecularly selective membrane (MSM) biorecognition based on MIPs, coupled with a laser-patterned microcapillary channel array for sample acquisition, and a hydrophobic protection layer. The device is fabricated on a styrene-ethylene-butylene-styrene (SEBS) elastomer substrate to allow flexibility and stretchability of the wearable sensor.

The crucial aspect of the sensor, artificial recognition, is achieved by copolymerizing a functional monomer and cross-linker in the presence of the analyte (in this case, cortisol), which acts as a molecular template (*34*). After elution of the analyte from the polymer product, binding sites complementary in size and shape to the template are revealed, creating a molecular memory on the surface that allows specific rebinding of the analyte (*35*). The recognition sites obtained in this manner have binding properties akin to those demonstrated by antibody-antigen systems. Furthermore, this artificial recognition technique displays a clear advantage over real antibodies: They are intrinsically stable, are robust, and can be easily integrated in an electronic device, facilitating their application in various environments, such as any bodily fluids, or at high temperatures, which makes them ideal recognition elements for wearable sensors. The working principle of the functionalization of the OECT with molecular recognition is as follows: The MSM is interposed between the gate electrode and the channel and is ion-permeable in the absence of the analyte of interest, giving rise to a large change in source-drain current (ΔI_{SD}) upon gating of the OECT channel (V_G = 0.2 V versus Ag/AgCl). In the presence of the analyte, the membrane pores become sealed and block ion motion to the channel, strongly reducing the measured ΔI_{SD} of the OECT channel, thereby giving rise to a sensing event. We demonstrate this principle by fabricating OECT-based sensors that sense cortisol levels in physiologically relevant conditions. Both ex situ and wearable MS-OECTs show a log-linear response for cortisol concentrations ($C_{cortisol}$) in the range of 0.01 to 10.0 μM with sensitivity of 2.68 μA dec^{-1} (current per order of magnitude change in $C_{cortisol}$) and high selectivity against cortisol's structural analogs, which are found in sweat, that could interfere.

Sensor fabrication and characterization

Optimization of the MIP

To optimize the MIP formulation for the ideal MSM, we studied the effect of polymerization conditions, ratio of template/monomer/cross-linker to initiator concentrations, and reaction medium (solvent). We based our first synthesis on literature specific to the formulation of MIPs designed for cortisol, and further extended the tests to some new formulations as described in Table 1 (*36*). Once synthesized, the imprinting efficiencies of each MIP formulation were determined by combining each polymer with the OECT sensor device and measuring the response to increasing concentrations of cortisol in an artificial sweat solution (90 mM NaCl, 10 mM NaCl, 5 mM NH_4Cl, and 0.1 mM $MgCl_2$) (Table 1 and figs. S1 to S5). For the optimization, we investigated several key factors that influence the quality of the MIP. For instance, the selection of the solvent is crucial due to its considerable effect on polymer morphology (*34*). Usually, porogenic solvents lead to a higher inner surface area and porosity due to high vapor pressure, which gives easier access to the molecular cavity that is formed after template removal (*37*). Among three different solvents, we observed that dichloromethane (DCM) showed better performance over acetonitrile and methanol to make the polymer more porous, and as a result more sensitive, by providing more binding sites. The cross-linker is another key parameter for MIP quality because the polymer must have a sufficient degree of cross-linking for the binding sites to remain intact after the template is removed. Furthermore, if the binding sites are too soft, they might also bind molecules that are similar to the template. All polymerizations were initiated photochemically by ultraviolet (UV) irradiation, which is preferred over thermal initiation due to potential chemical reactions or degradation of the template. Overall, D1630 (Table 1) was identified as the optimal MIP formulation for our wearable cortisol sensor due to its high sensing factor and specific surface area.

After finding the ideal MIP processing conditions, we investigated surface characteristics, surface morphology, and porosity of the MIPs. To characterize the effectiveness of the molecular templating and provide a meaningful control, we produced NIPs using the same conditions as the MIPs, except in the absence of the cortisol molecular template. The MIP (D1630) and NIP (D1630C) were characterized by AFM and SEM (Fig. 1, B to G, and figs. S16 and 17). The characterization shows that the MIP has a porous structure with nanopores, while the NIP displays significantly less porosity. Both characterization methods show consistently that the MIP has mainly nanopores (≤10 nm) and mesopores (10 nm ≤ diameter ≤ 100 nm). The NIP structure, on the other hand, is dominated by relatively bigger macropores (≥100 nm). The SEM micrographs of both the MIP and NIP

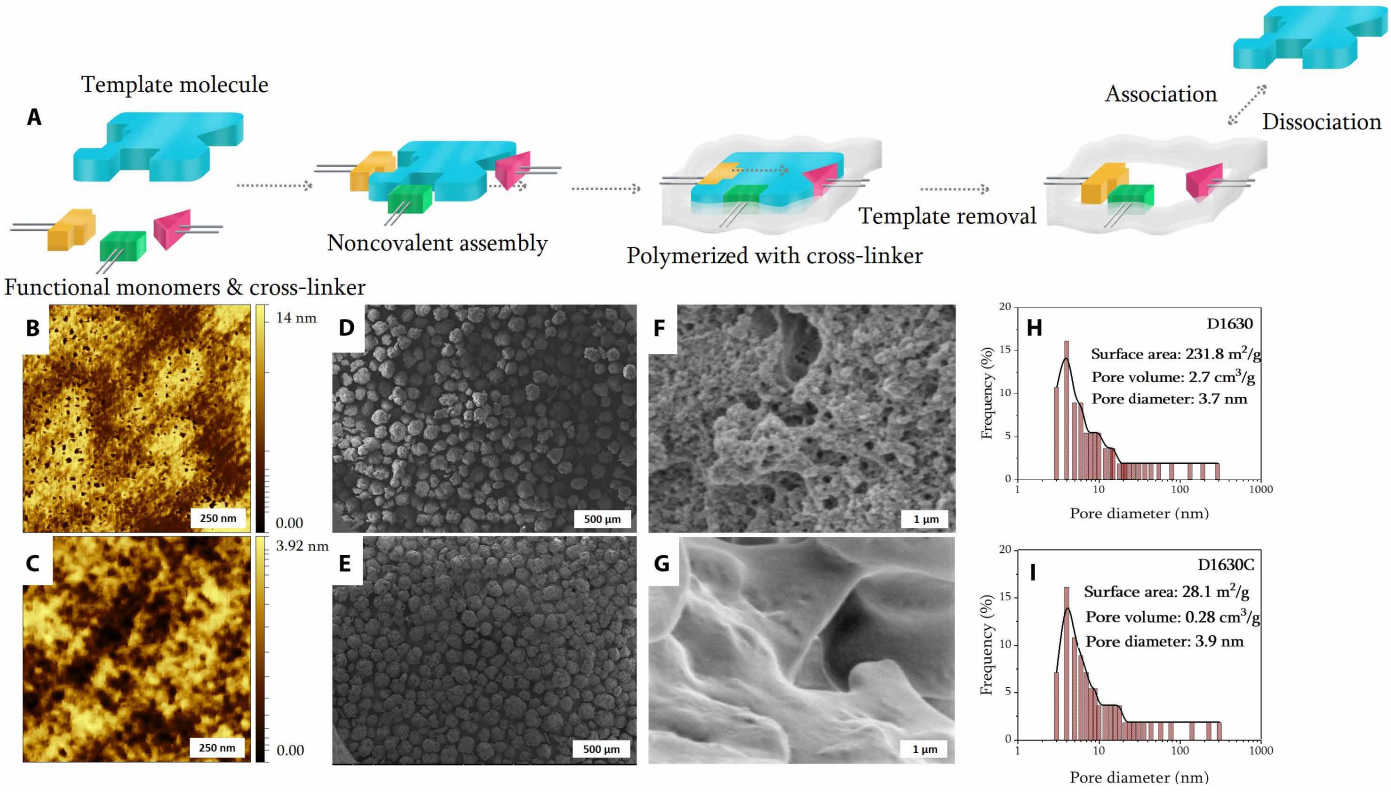

Fig. 1. Schematic representation of noncovalent imprinting process and corresponding surface characterizations by microscopy. (**A**) Molecular memory is introduced on the sensor surface by copolymerizing functional monomer and cross-linker in the presence of the analyte, which acts as a molecular template. After elution of the analyte, complementary binding sites are revealed complimentary in size and shape to template by creating molecular memory on the surface that allows specific rebinding of the target molecule. The recognition sites obtained in this manner have binding affinities approaching those demonstrated by antibody-antigen systems. Tapping-mode atomic force microscopy (AFM) analysis of cortisol-selective polymer (**B**) and its corresponding control (**C**). Scanning electron microscopy (SEM) images of cortisol-selective polymer (**D** and **F**) and its control (**E** and **G**) with two different magnifications. Pore size distribution for cortisol-imprinted (**H**) and nonimprinted polymers (NIPs) (**I**). The BJH method was applied to calculate pore size distribution from experimental isotherms using the Kelvin model of pore filling. The method applies only to the mesopore and small macropore size range.

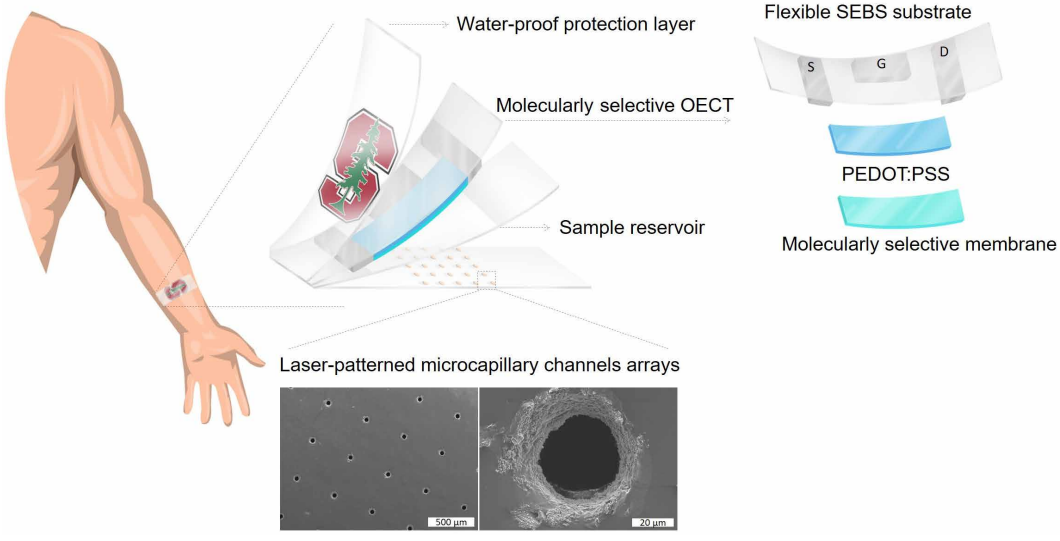

Scheme 1. Schematic drawings of the patch-type wearable cortisol sensor. The integrated wearable sensor consists of several important layers from bottom to top as follows: (i) laser-patterned microcapillary channel arrays for sweat acquisition (bottom layer), (ii) sample reservoir to assist sample delivery, (iii) sensor layers composed of the OECT device on the flexible SEBS elastomer substrate with the PEDOT:PSS semiconductor layer and the MSM, and (iv) polyethylene-based hydrophobic protection layer.

Table 1. Optimization conditions. Formulations used to design cortisol-selective polymers. The values are calculated by taking the ratio of slope of each sensor calibration curve for each molecularly imprinted and nonimprinted control polymer (Fig.3, B and C, and figs. S1 to S5). The starting concentration of cortisol is 0.2 mmol in each condition. Control polymers are not included in the table; they were prepared exactly as corresponding selective polymer but without the template. AIBN, azobisisobutyronitrile.

Membrane	Monomer	Cross-linker	Initiator	Solvent	Ratio*	Conditions	Sensing factor†
A1618	MAA	EDMA	AIBN	Acetonitrile	1:6:18	UV, 4°C, 30 hours	4.2
M1618	MAA	EDMA	AIBN	Methanol	1:6:18	UV, 4°C, 30 hours	5.1
D1618	MAA	EDMA	AIBN	DCM	1:6:18	UV, 4°C, 30 hours	5.4
D1630	MAA	EDMA	AIBN	DCM	1:6:30	UV, 4°C, 30 hours	10.1
D1660	MAA	EDMA	AIBN	DCM	1:6:60	UV, 4°C, 30 hours	2.2
D1630RT	MAA	EDMA	AIBN	DCM	1:6:30	UV, room temperature, 30 hours	6.7

*Molar ratio of template/functional monomer/cross-linker. †Calculated based on each sensor device's performance to express imprinting efficiency.

show the formation of large globular-shaped particles resulting from the polymerization process. The formation of nanopores in the MIP is a result of the increased solubility of the polymer in the presence of the template, which delays precipitation of the highly cross-linked gel (note S1). In addition to microscopy and porosity measurements, the specific surface areas were determined by Brunauer-Emmett-Teller (BET) measurements (table S1). All adsorption-desorption isotherms of the MIP and NIP polymers show the presence of mesopores and have a small hysteresis between adsorption and desorption curves due to capillary condensation. The pore size distribution for all MIPs and NIPs was calculated (Fig. 1, H and I). The Barrett-Joyner-Halenda (BJH) method was applied to calculate the pore size from experimental isotherms using the Kelvin model of pore filling.

Microfluidic sample acquisition

The second key requirement for the successful implementation of wearable sensors is to acquire a sufficient amount of sample to assess analyte concentration while maintaining direct and continuous sampling to reduce environmental factors, which mainly cause contamination and uncontrolled delivery (*5*). For all on-body biosensors, bodily fluids must be either collected on or delivered to the sensor surface with minimum delay to yield an accurate sensor response (*14*). Here, we achieve such rapid sampling by using microfluidic technology. With microfluidics, very small sampling volumes can be collected at the sensor surface to generate the same quality of response compared to bulk solution analysis. The main challenge in the design of all on-body biosensors is the low sweat output from the skin surface (*38*). We generate passive capillary-driven fluid control by laser patterning 20-μm-wide channels on 80-μm-thick single-sided medical-grade tapes connected to the sensor by a double-sided medical-grade tape, which serves as a sample reservoir that can accommodate sweat samples of more than 100 μl (Scheme 1 and fig. S20). The assembly of these two components forms the acquisition layer, which both prevents sensor contamination and provides the precise delivery of sample directly to the sensor interface. Considering a sweat generation rate of 1 to 100 nl/min per gland for an average healthy person with a gland density of 100 glands/cm^2 and a large sensor area of 0.8 cm^2, the channels absorb about 10 to 50 μl of sweat, which is sufficient to provide stable sensor readings using the proposed design.

Membrane-integrated device characterization

A critical aspect in the design of molecularly selective sensors is to find an appropriate way of interfacing the MIP with the transducer. Directly depositing the MIP onto the PEDOT:PSS channel results in selectivity loss due to direct diffusion of molecules to the transducer surface (fig. S10). Here, we entrap the MIP into an inert polymeric medium, which serves as a glue and flexible medium (*39*, *40*). We incorporated the cortisol-selective MIP (40% by weight) into a plasticized poly(vinyl chloride) (PVC) matrix to form the MSM, which regulates ion transport to the PEDOT:PSS channel (see Materials and Methods).

To understand the effect of integration of the MSM, we measured the device characteristics before and after introducing it on the PEDOT:PSS-based OECT channel. The addition of the MSM to the PEDOT:PSS device reduces the peak OECT transconductance (g_m) by a factor of ~3, with optimal performance still at V_G = 0.2 V versus Ag/AgCl (Fig. 2, B to E). The MSM acts as an ionic barrier and is therefore expected to reduce the overall g_m of the device because of the higher impedance between the gate and channel. This performance reduction, however, does not prevent efficient OECT operation as a sensor.

The electrochemical performance of the MS-OECT sweat-based cortisol sensor was first evaluated in vitro without using sample acquisition and protection layers (Fig. 3A). The electroanalytical performance of MS-OECT devices was investigated by measurements of the ΔI_{SD} response as a function of cortisol concentration (Fig. 3B). We compared the response of the MS-OECT to an OECT device with a nonselective membrane prepared using the NIP under the same conditions (NS-OECT). The MS-OECT exhibited fast response times of just under 1 s to reach steady-state current, while the NS-OECT failed to respond to changes in cortisol concentration. The devices are calibrated by plotting the value of the ΔI_{SD} as a function of the cortisol concentration in solution. To show the reversibility of the binding process, we designed cortisol-sensing experiments with decreasing and increasing cortisol concentrations on the same device. The device shows continuous and stable responses in both low-to-high and high-to-low concentration regime (Fig. 3C and figs. S6 and S7). We tested the device response in the range of 0.0001 to 500 μM. First, the sensor response was tested from low to high concentrations, and then after the full range of measurements was complete, the sensor

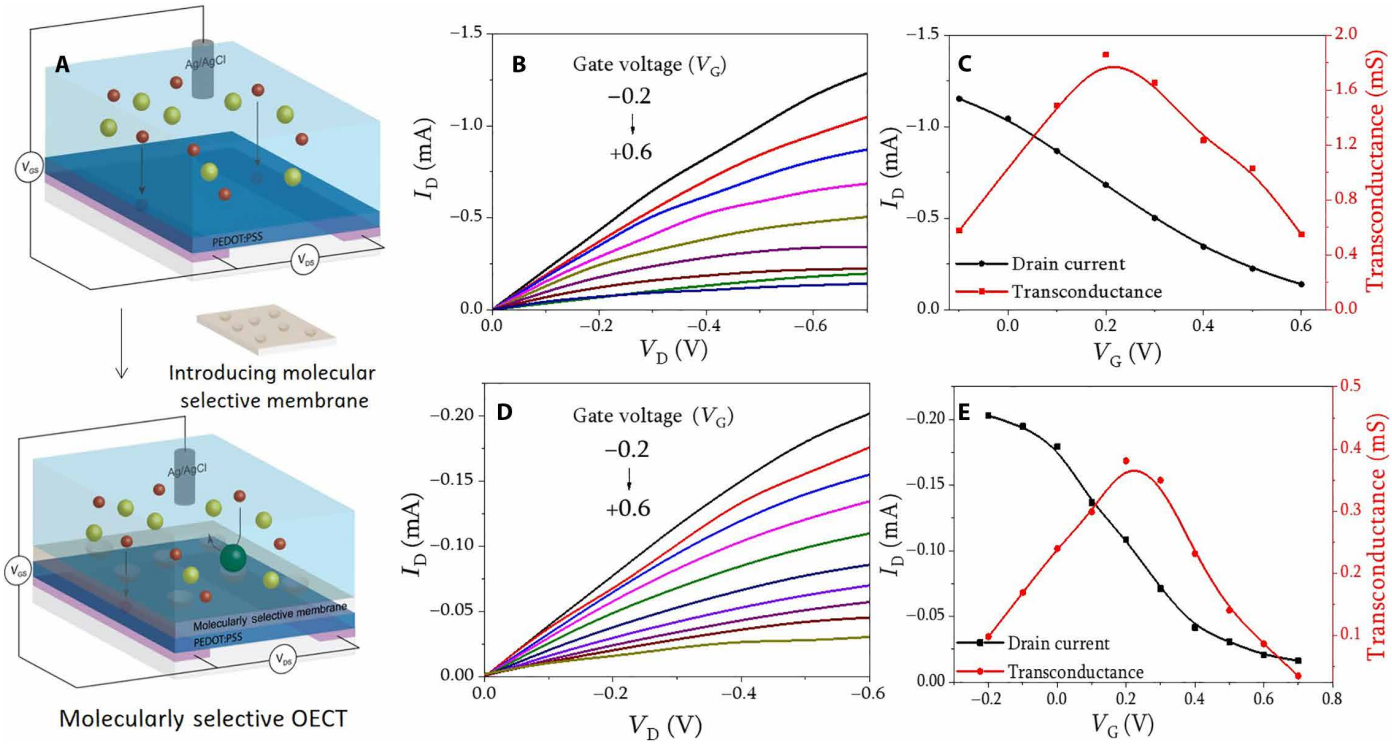

Fig. 2. Schematic representation of membrane integration and device characteristics. (**A**) Schematic drawing of integration of MSM to OECT device consisting of PEDOT:PSS channel coated on an indium tin oxide glass substrate with the cortisol-selective membrane separating the PEDOT:PSS channel from the electrolyte solution, gated with an Ag/AgCl electrode. Device characteristics demonstrated by output and transfer curves before (**B** and **C**) and after (**D** and **E**) membrane integration. The output and transfer curve measurements were conducted in artificial sweat solutions.

surface was rinsed with washing solution [acetic acid/ethanol (8:2, v/v)] and sonicated for 30 s to regenerate the sensor surface. The cortisol concentration was successively reduced from 500 to 0.0001 μM. The device showed a stable response in both directions. We also designed an experiment to understand device behavior when the sensor is saturated. We increased the cortisol concentration about 10 times on the same device (up to 5 mM). We then gradually decreased the cortisol concentration from 5 mM to 0.001 μM. In this condition, the device does not respond to decreasing concentrations of cortisol. These experiments show that device saturation and molecular binding play an important role in the sensing process. However, our device still shows good sensing characteristics in the range of physiological (0.1 to 1.0 μM) cortisol concentration, which is very far from the saturation level. The selectivity and specificity of the MS-OECT device were also evaluated in the presence of structural analogs to cortisol such as progesterone, cortisone, and testosterone. The cortisol-imprinted membrane does not respond to these structural analogs (Fig. 3D and fig. S16), demonstrating good specificity.

Stability of the MS-OECT under mechanical stress

Because the human epidermis regularly experiences deformation due to bodily movement, which is usually a cause of concern for wearable devices, we performed several ex situ mechanical tests such as bending and stretching of the device in artificial sweat containing a constant concentration of cortisol (0.5 μM). Accordingly, the sensor device was flexed to a 90° angle for 1000 iterations, while measurements of ΔI_{SD} were conducted after 10, 100, 500, and 1000 bending cycles. The results were compared with an unflexed device (fig. S17), showing that the device was not affected in the first 10 bending cycles. After 100 to 500 bending cycles, the device performance diminished insignificantly (≤5%). The bending test was followed by stretching the sensor in various strain percentages ranging from 10 to 100%. The results demonstrate that the sensor response remained uniform up to 40% stretching; however, when 100% stretching was applied, both the substrate and sensor interface were visibly deformed, and the sensor response decreased significantly (≥70%). Nevertheless, considering the natural stretching of the forearm (≤20%), which is the location where the sensor will be placed, our device shows promise for on-body sensing.

Evaluation of the sensor performance

Skin-like microfluidic system for in vitro evaluation

To test the sample acquisition layer-integrated device for real sample analysis, we designed a skin-like flexible microfluidic device based on poly(methyl methacrylate) (PMMA) to mimic the real-time sensing environment (see Materials and Methods) (Fig. 4A) before performing on-body measurements. First, both the MS-OECT and NS-OECT devices were tested in artificial sweat (Fig. 4, B and C). The artificial sweat samples were delivered to the microfluidic channel with a syringe. After injecting the sample, mechanical pressure was applied to the sample reservoir to accelerate the delivery process. The sensing and calibration curves for artificial sweat sensing are shown in Fig. 4C. The results demonstrate that the measurements on the skin-like microfluidic device have similar characteristics as the ex situ analysis (Fig. 3D). The same system was used to perform a real sample analysis.

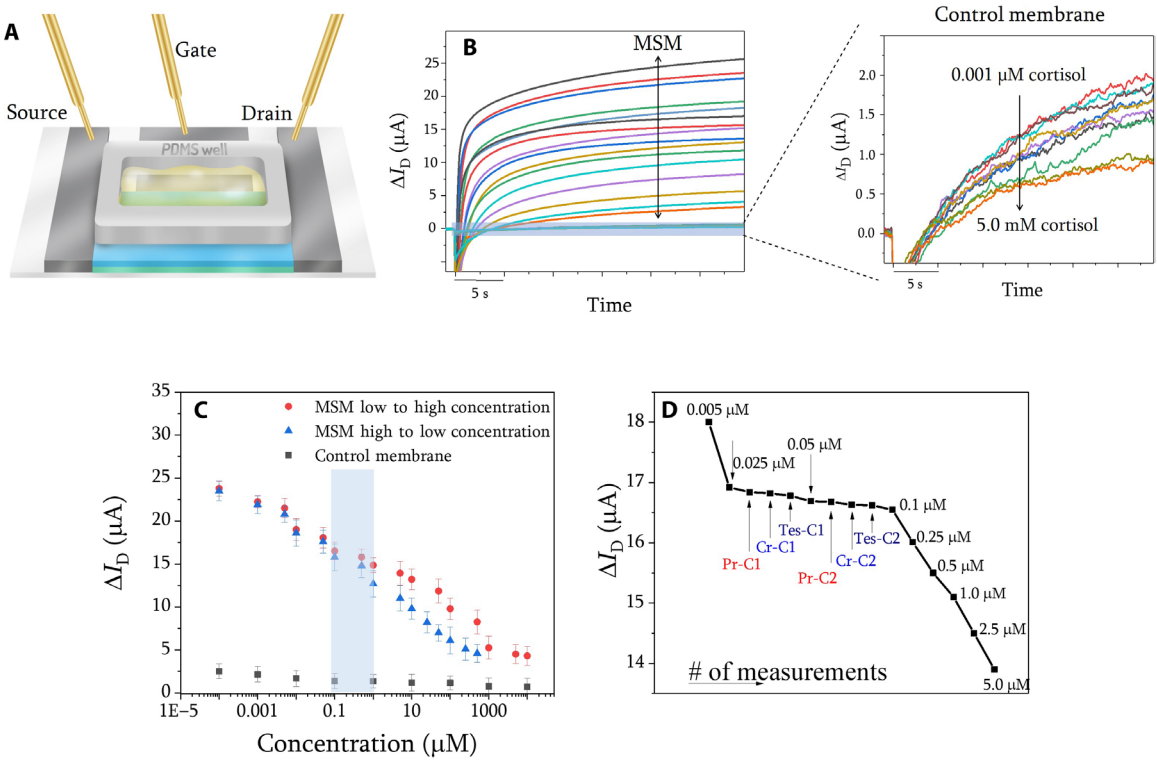

Fig. 3. Testing of MS-OECT device for ex situ analysis. (**A**) Schematic drawings of planar-gated MS-OECT device on the SEBS substrate for drain current measurements. PDMS, polydimethylsiloxane. Ex situ measurement for MSMs (inset: control membrane) (**B**) and their corresponding calibration curves (the calibration curve for high-to-low concentration is based on fig. S6B, and the highlighted area shows the physiological range of cortisol in human sweat) (**C**). The measurements were conducted in artificial sweat with increasing concentrations of cortisol. The selectivity of the MS-OECT device was evaluated in the presence of structural analogs of cortisol including progesterone, cortisone, and testosterone in artificial sweat. The measurement was started with 0.005 mM cortisol, and it was gradually increased up to 5.0 μM. The concentrations of interferent were increased step-wise for progesterone (Pr-C1, 0.025 μM; Pr-C2, 0.5 μM), cortisone (Cr-C1, 0.025 μM; Cr-C2, 0.5 μM), and testosterone (Tes-C1, 0.025 μM; Tes-C2, 0.5 μM) to ensure that they do not involve a binding process (**D**). The drain current measurement of each run is shown in fig. S25.

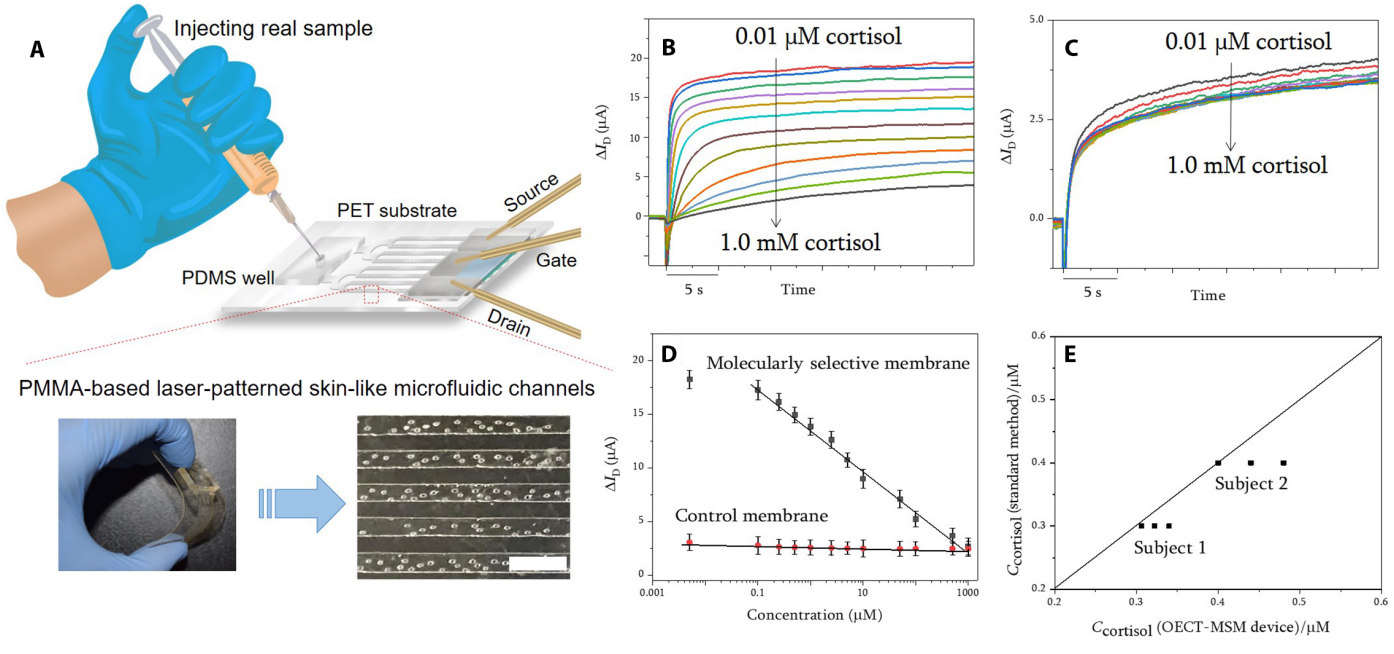

Fig. 4. Ex situ real sample analysis using skin-like microfluidic device. (**A**) Schematic drawing of skin-like microfluidic device with a photograph of the device while being flexed, and an optical micrograph of the device surface. Scale bar, 500 μm. Drain current measurements of molecularly selective (**B**) and control (**C**) membrane-integrated devices for ex situ analysis and their corresponding calibration curves (**D**). (**E**) Real sample analysis and comparison with standard cortisol ELISA for two subjects for three repetitive measurements for each subject.

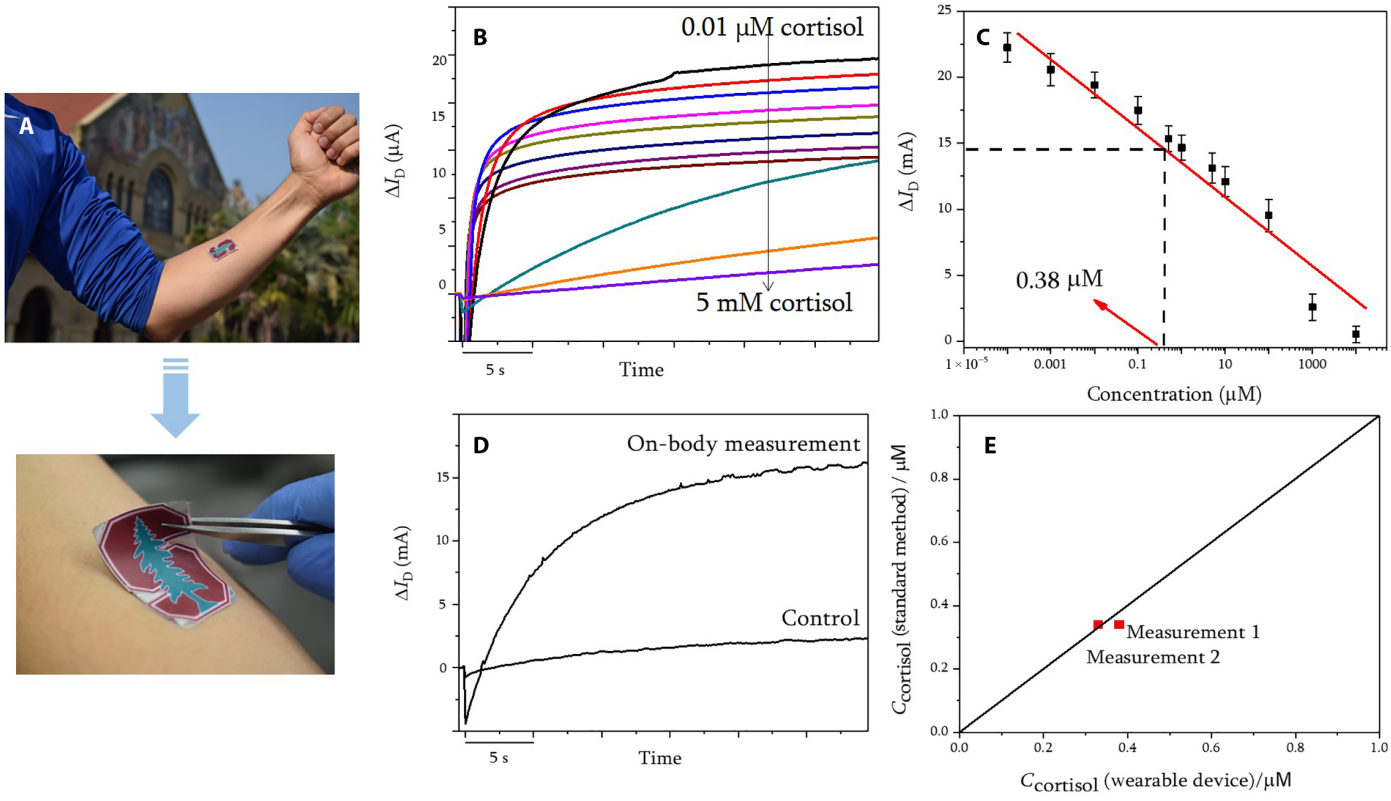

Fig. 5. Analytical performance of the wearable cortisol sensor. (**A**) MS-OECT device applied to male volunteer's forearm. The device was tested by spraying artificial sweat with increasing concentrations of cortisol on volunteer's forearm and measuring the corresponding output current (**B**) to obtain a calibration curve (**C**). (**D**) The real-time response of both the molecularly selective and control devices was measured after completing physical exercise by mounting electrical contacts to the wearable sensor device. The cortisol response was recorded using the output measurement, and data were represented as a change of drain current (ΔI_D) at a low voltage, which substantially reduces the possibility of electrical shock. The cortisol concentration was measured using sweat directly from the skin, and the results were compared with the best fit of (B) [relative standard deviation (RSD) = 35% for n = 2]. RSD, relative SD. (**E**) The data obtained showed a good correlation with the standard cortisol ELISA method for cortisol detection with an RSD of 5% for two measurements.

Sweat samples were collected from two human subjects using a sweat collector placed on the forearm, firmly strapped in place during exercise. These fresh real sweat samples (50 to 100 μl) were delivered to the skin-like microfluidic device using a syringe. The analysis was conducted using the standard addition method. Briefly, the standard addition method is performed by step-wise increasing concentrations (30% increment in each addition) of cortisol to the unknown concentration of the real samples on the same sample to assess matrix effects in the analytical measurement. Figure 4E shows the comparison of the cortisol content of the sweat of two participants. We compare the standard addition test done with MS-OECTs to the standard cortisol enzyme-linked immunosorbent assay (ELISA) test. The measurements of the cortisol-selective membrane-integrated sensor are correlated with those obtained with the ELISA method. We thus conclude that our sensors can be further used for the on-body analysis of cortisol.

On-body cortisol measurement with a patch-type wearable sensor

Before on-body real sample analysis using the molecularly selective wearable cortisol sensor, we evaluated sample acquisition efficiency and the rate of sample collection through the microfluidic channels. We compared the laser-patterned acquisition layer with a simple 0.2 cm × 0.2 cm hole punch (aligned with the sensor interface) in the medical tape. Tests were performed using 100 μl of artificial sweat solution applied to the forearm. Measurements of the ΔI_{SD} response were performed for each sample acquisition method (fig. S21). The device that is integrated with the mechanical punch as an acquisition layer displays poor sample collection and could not generate significant signal until 6 min after application of the sensor. The device integrated with the laser-patterned acquisition layer, on the other hand, immediately delivered the artificial sweat samples to the sensor interface and remained stable over 10 min. Thus, capillary channels dramatically improve sample delivery. We tested the sensing dynamics by spraying constant concentrations of artificial sweat to the forearm with increasing cortisol concentrations ranging from 0.001 to 1.0 mM. The measurements were conducted by measuring each concentration separately using the same device (Fig. 5, A and B). Before each measurement, the forearm was cleaned with an ethanol solution and allowed to dry for 5 min before spraying a new sample. The device shows linear response over a wide range of cortisol concentrations. The results show close correspondence between sprayed sample and standard ELISA measurements (Fig. 4, B to D).

For the on-body real sample analysis, the MS-OECT wearable device was applied to a volunteer's forearm to assess cortisol concentration after completing a 20-min intensive outdoor running exercise. The cortisol response was recorded by measuring ΔI_{SD} for an applied V_G = 0.2 V versus Ag/AgCl at the end of the exercise. To validate the selectivity of the wearable sensor to measure cortisol binding, a nonfunctionalized NS-OECT device was also applied to

the same subject's forearm within 2 min of the initial measurement to serve as a control sensor. Medical-grade adhesive was used to seal the electrical connection to the source-drain and gate connections. The low supply voltage is advantageous because it minimizes the possibility of electric shock. Figure 5C displays the real-time monitoring of the ΔI_{SD} data for both the MS-OECT (black curve) and NS-OECT control device (red curve). The MS-OECT demonstrated binding affinity to cortisol in sweat, while the control device did not show any binding event and corresponding signal. Moreover, the background I_{SD} and the corresponding noise level are low. The low noise level indicates the reliability of the ΔI_{SD} measurement, the electrical contacts, and the sensor interface. To validate the cortisol-sensing measurement, we compared the results with on-body sprayed samples (Fig. 5B) to determine the exact concentration of cortisol. The cortisol concentration was calculated by interpolating the ΔI_{SD} value of the on-body calibration curve obtained with the sprayed samples and was calculated to be 0.38 μM. To further validate the measurement, we used a standard cortisol ELISA test on a sample collected from the same volunteer during exercise, before conducting our real sample analysis with the MS-OECT. Figure 5D indicates a strong correlation between the in vitro response and the on-body measurements. Both measurements were performed twice under the same conditions. This agreement between in vitro and on-body measurements may be attributed to the successful on-body sweat collection methodology via the laser-patterned microcapillary channel interface and the quality of the sensor interface.

DISCUSSION

In summary, we have demonstrated the integration of an artificial receptor as a biomimetic polymeric membrane for stable and selective molecular recognition using OECTs to produce a wearable sweat diagnostics platform for real-time analysis of the human stress hormone cortisol. This wearable sensing device for cortisol detection was realized using a conductive polymer channel functionalized with a cortisol-selective membrane produced on a flexible and stretchable elastomeric substrate. The molecularly selective polymer-based membrane shows high chemical and physical stability at body temperature, as well as resistance to physical deformation. The presented sensor tolerates mechanical testing such as bending and stretching in conditions similar to those found in the normal range of motion of the human epidermis. Moreover, we used a simple strategy to generate a passive fluid control system consisting of a laser-patterned microcapillary channel array that provides fast and precise delivery of sweat directly to the sensor interface. The resulting wearable sensor was used for measuring cortisol concentration in a real human sweat sample collected during exercise. Considering that traditional blood analysis is often used for cortisol sensing, the wearable device provides many advantages including noninvasiveness, ease of operation, and user comfort. The initial results suggest that the design principles presented here can be adapted for the selective detection of various other molecules, especially noncharged biomolecules and hormones. Moreover, future efforts will be aimed at miniaturizing the device, combining different sensing interfaces for multiplexing, data evaluation, processing and transmission of the results to a user interface, noninvasive sweat induction, and harvesting energy directly from bodily fluids to power the device.

MATERIALS AND METHODS

Preparation of cortisol-selective MIPs

All MIPs were synthesized by bulk polymerization. For all polymerization conditions, 0.2 mmol of the template (cortisol) was used. The initiator 2,2′-azobis (2-methylpropionitrile), azobisisobutyronitrile (AIBN) [0.2 mole percent (mol %) of template], methacrylic acid (MAA) functional monomer (1.2 mmol), and ethylene glycol methacrylate (EDMA) cross-linker (from 3.6 to 12 mmol depending on optimization parameters) were dissolved in corresponding solvent the reaction chamber was sealed and then the mixture was degassed with N_2(g) for 10 min. The polymerization was initiated by UV irradiation at either room temperature or 4°C for 30 hours. The control NIPs were prepared by following the same conditions, except neglecting to add the template molecules to the reaction chamber. After mechanically grinding the as-synthesized polymer, they were processed by washing in acetic acid/methanol mixture (8:2, v/v). The washing solution was applied to polymers by first dispersing the particles in the centrifuge tube, shaking for 30 min, and then centrifuging at 1000 rpm for 15 min. This process was repeated five times successively for each polymer, and all particles were dried at vacuum overnight.

Device fabrication

The SEBS substrate was prepared successively by dissolving the SEBS polymer in toluene (200 mg/ml) and curing in a petri dish overnight. After obtaining a thin elastomer film (100 μm thick) as a flexible and stretchable substrate, it was cleaned by handwashing with soap followed by sonication in baths of methanol and then isopropanol for 10 min each. The substrates were treated with UV-ozone for 30 min. Ag/AgCl paste was brush-printed for gate, source, and drain contacts, and the whole substrate was baked at 110°C for 20 min to cure the conducting contacts. After stabilizing the conducting paste, drain source and gate contacts were masked to spin coat the first layer of PEDOT:PSS. The PEDOT:PSS blend was prepared by adding ethylene glycol (6 volume %) (Sigma), (3-glycidyloxypropyl)trimethoxysilane cross-linking agent (1 volume %), and dodecylbenzenesulfonic acid (one drop per 10 ml) to a stock Clevios PH 1000 PEDOT:PSS solution (Heraeus). The PEDOT:PSS solution is then spin-coated onto clean substrates at 2000 rpm to achieve a film thickness of approximately 100 nm. The molecularly selective and/or control membranes were coated on top of PEDOT:PSS by spin coating a tetrahydrofuran (2 ml) mixture containing a high–molecular weight PVC (50.0 mg), the bis(2-ethylhexyl) plasticizing solvent mediator (120.0 μl), and the anion excluder potassium tetrakis(4-chloropheny1) borate (15.0 mg). We varied the composition of MIP in the PVC matrix (10, 25, and 40% by weight) and observed the highest selectivity and sensitivity with 40 weight % (wt %) MIP content. Further increase of the concentration of MIP in PVC resulted in a highly dense, slurry-like mixture that could not be processed for further applications. After coating the membrane, contacts were exposed to the electrode connection for further characterization.

Device characterization

All output, transfer, and drain current measurements were performed with the Keithley 2612 SourceMeter using custom LabVIEW software. All voltammetric measurements were carried out using a BioLogic SP-200 potentiostat. Cyclic voltammetry measurements were performed in conventional three-electrode setup, where Ag/AgCl was used as the reference electrode, the platinum wire as the auxiliary counter electrode, and the whole device as the working electrode.

BET measurement

The specific surface area of the different templates was evaluated by nitrogen physiosorption using a BET Quantachrome Autosorb iQ3 instrument. The samples were degassed under vacuum at 80°C for 6 hours before analysis. The pore size was determined using the desorption isotherms in a relative pressure window of 0.35 to 0.99 and following the BJH approach.

Collection of real samples for ex situ and on-body measurements

The sweat samples used in all experiments were collected with a Macroduct sweat collector placed on the skin and firmly strapped in place during outdoor running exercises. Sweat secreted by the sweat glands was forced from the ducts under hydraulic pressure and flowed between the skin and the concave under the surface of the collector and into the micropore tubing spiral. The sweat samples were collected from healthy human subjects. The on-body measurements were performed in compliance with institutional review board guidelines. All subjects gave written, informed consent before participation in the study.

Fabrication of skin-like microfluidic device

The laser-patterned microfluidic device was fabricated using a multilayered fabrication approach. The base layer of the device consisted of a 125-μm-thick PMMA foil, while the skin-like laser pattern was defined on a 50-μm-thick PMMA foil. Laser ablation of 60 μm through holes on PMMA was performed using a high-power density focusing optics (VLS6.60, Universal Laser Systems) to achieve high resolution during laser ablation. A single layer of a double-sided medical-grade pressure-sensitive adhesive (PSA) was laser cut to define the branched microfluidic structure. The three layers were then manually aligned and laminated together to obtain stable and irreversible bonding of the PSA with the top and bottom PMMA layers.

Fabrication of laser-patterned microcapillary channels

Laser-patterned microfluidic channels were introduced into the medical-grade tape using a femtosecond laser (500 mW, 808 nm, 1 kHz; Spectra-Physics) to locally etch through the thickness of the tape without melting using a spot size of approximately 20 μm. A shutter was used to block the beam as the sample was translated by 100 μm in the x and y axes to fabricate an array of microfluidic pores.

Setup for on-body testing

Double- and single-sided medical-grade tapes were integrated with the MSM-based sensor surface after laser patterning to provide efficient sweat collection via capillary action. These laser-patterned channels and reservoir layers absorb and collect sweat to provide stable and reliable sensor readings while also preventing direct mechanical contact between the sensor and skin. During on-body tests, the newly generated sweat would fill the reservoir and was delivered to the sensor interface. The on-body measurement results were also consistent with ex situ tests using freshly collected sweat samples.

As a safety note, it is highly advised that the electrochemical measurement (output measurement) apparatus should be voltage- and current-limited to reduce the likelihood of unintentional electric shock.

Standard measurements using cortisol ELISA

The Human Cortisol ELISA Kit (Biotang Inc.) was used for the quantitative determination of the concentrations of human cortisol in sweat. The kit assays human cortisol in the samples by double-antibody sandwich ELISA. The human cortisol antibody-coated microplate was used. For the binding, biotinylated cortisol antibody, the horseradish peroxidase (HRP)– streptavidin enzyme conjugate was added to the wells. After washing to remove the unbound antibody enzyme reagent, the tetramethylbenzidine (TMB) substrate was added. The TMB substrate produced a blue color when the HRP enzyme was catalyzed. After reaching the desired color intensity, the reaction was terminated by the addition of an acidic stop solution, which changed the solution color from blue to yellow. The absorbance at a wavelength of 450 nm was measured by the microwell reader and the concentration of cortisol was calculated according to the standard curve. Standard kits and solutions were kept at 4°C unless otherwise used.

SUPPLEMENTARY MATERIALS

Supplementary material for this article is available at http://advances.sciencemag.org/cgi/content/full/4/7/eaar2904/DC1

Supplementary Materials

Fig. S1. Ex situ device testing for A1618 and A1618C.
Fig. S2. Ex situ device testing for M1618 and M1618C.
Fig. S3. Ex situ device testing for D1618 and D1618C.
Fig. S4. Ex situ device testing for D1630 and D1630C.
Fig. S5. Ex situ device testing for D1630RT and D1630RTC.
Fig. S6. Reversibility test for unsaturated device.
Fig. S7. Reversibility test for saturated device.
Fig. S8. SEM characterization of MIP.
Fig. S9. SEM characterization of NIP.
Fig. S10. Drain current measurements without PVC matrix.
Fig. S11. Drain current measurements in 10% PVC matrix.
Fig. S12. Drain current measurements in 25% PVC matrix.
Fig. S13. Washing tests by cyclic voltammetry.
Fig. S14. Diffusion characteristics of the MS-OECT.
Fig. S15. Diffusion characteristics of the NS-OECT.
Fig. S16. Selectivity tests.
Fig. S17. Bending tests.
Fig. S18. Stretchability tests.
Fig. S19. The reusability tests.
Fig. S20. SEM characterization of microchannel arrays.
Fig. S21. The performance of acquisition layer.
Fig. S22. The reusability test for on-body real sample analysis.
Table S1. BET characteristics.
Note S1. Nanopore formation in MIP.
Note S2. Rationale for MIP design.
Note S3. Diffusion characteristics of MSM.

REFERENCES AND NOTES

1. A. N. Sekretaryova, M. Eriksson, A. P. F. Turner, Bioelectrocatalytic systems for health applications. *Biotechnol. Adv.* **34**, 177–197 (2016).
2. H. Lee, C. Song, Y. Seok Hong, M. Sung Kim, H. R. Cho, T. Kang, K. Shin, S. H. Choi, T. Hyeon, D.-H. Kim, Wearable/disposable sweat-based glucose monitoring device with multistage transdermal drug delivery module. *Sci. Adv.* **3**, e1601314 (2017).
3. A. P. F. Turner, Biosensors: Sense and sensibility. *Chem. Soc. Rev.* **42**, 3184–3196 (2013).
4. D. Son, J. Lee, S. Qiao, R. Ghaffari, J. Kim, J. E. Lee, C. Song, S. J. Kim, D. J. Lee, S. W. Jun, S. Yang, M. Park, J. Shin, K. Do, M. Lee, K. Kang, C. S. Hwang, N. Lu, T. Hyeon, D. H. Kim, Multifunctional wearable devices for diagnosis and therapy of movement disorders. *Nat. Nanotechnol.* **9**, 397–404 (2014).
5. J. R. Windmiller, J. Wang, Wearable electrochemical sensors and biosensors: A review. *Electroanalysis* **25**, 29–46 (2013).
6. T. Q. Trung, N.-E. Lee, Flexible and stretchable physical sensor integrated platforms for wearable human-activity monitoring and personal healthcare. *Adv. Mater.* **28**, 4338–4372 (2016).
7. G. Schwartz, B. C.-K. Tee, J. Mei, A. L. Appleton, D. Hwan Kim, H. Wang, Z. Bao, Flexible polymer transistors with high pressure sensitivity for application in electronic skin and health monitoring. *Nat. Commun.* **4**, 1859 (2013).

8. J. Young Oh, S. Rondeau-Gagné, Y.-C. Chiu, A. Chortos, F. Lissel, G.-J. N. Wang, B. C. Schroeder, T. Kurosawa, J. Lopez, T. Katsumata, J. Xu, C. Zhu, X. Gu, W.-G. Bae, Y. Kim, L. Jin, J. Won Chung, J. B.-H. Tok, Z. Bao, Intrinsically stretchable and healable semiconducting polymer for organic transistors. *Nature* **539**, 411–415 (2016).
9. Y. Liu, J. J. S. Norton, R. Qazi, Z. Zou, K. R. Ammann, H. Liu, L. Yan, P. L. Tran, K.-I. Jang, J. W. Lee, D. Zhang, K. A. Kilian, S. Hee Jung, T. Bretl, J. Xiao, M. J. Slepian, Y. Huang, J.-W. Jeong, J. A. Rogers, Epidermal mechano-acoustic sensing electronics for cardiovascular diagnostics and human-machine interfaces. *Sci. Adv.* **2**, e1601185 (2016).
10. S. Kumar Kundu, S. Kumagai, M. Sasaki, A wearable capacitive sensor for monitoring human respiratory rate. *Jpn. J. Appl. Phys.* **52**, 04CL05 (2013).
11. S. Wen, H. Heidari, A. Vilouras, R. Dahiya, A wearable fabric-based RFID skin temperature monitoring patch, in *Proceedings of the 2016 IEEE SENSORS*, Orlando, FL, 30 October to 3 November 2016.
12. A. Casson, D. Yates, S. J. M. Smith, J. Duncan, E. Rodriguez-Villegas, Wearable Electroencephalography. *IEEE Eng. Med. Biol. Mag.* **29**, 44–56 (2010).
13. A. J. Bandodkar, J. Wang, Non-invasive wearable electrochemical sensors: A review. *Trends Biotechnol.* **32**, 363–371 (2014).
14. H. Lee, T. K. Choi, Y. B. Lee, H. R. Cho, R. Ghaffari, L. Wang, H. J. Choi, T. D. Chung, N. Lu, T. Hyeon, S. H. Choi, D. H. Kim, A graphene-based electrochemical device with thermoresponsive microneedles for diabetes monitoring and therapy. *Nat. Nanotechnol.* **11**, 566–572 (2016).
15. J. Heikenfeld Non-invasive analyte access and sensing through eccrine sweat: Challenges and outlook circa 2016. *Electroanalysis* **28**, 1242–1249 (2016).
16. S. Emaminejad, W. Gao, E. Wu, Z. A. Davies, H. Yin Yin Nyein, S. Challa, S. P. Ryan, H. M. Fahad, K. Chen, Z. Shahpar, S. Talebi, C. Milla, A. Javey, R. W. Davis, Autonomous sweat extraction and analysis applied to cystic fibrosis and glucose monitoring using a fully integrated wearable platform. *Proc. Natl. Acad. Sci. U.S.A.* **114**, 4625–4630 (2017).
17. W. Gao, H. Y. Y. Nyein, Z. Shahpar, H. M. Fahad, K. Chen, S. Emaminejad, Y. Gao, L.-C. Tai, H. Ota, E. Wu, J. Bullock, Y. Zeng, D.-H. Lien, A. Javey, Wearable microsensor array for multiplexed heavy metal monitoring of body fluids. *ACS Sens.* **1**, 866–874 (2016).
18. H.-J. Jang, T. Lee, J. Song, L. Russell, H. Li, J. Dailey, P. C. Searson, H. E. Katz, Electronic cortisol detection using an antibody-embedded polymer coupled to a field- effect transistor. *ACS Appl. Mater. Interfaces* **10**, 16233–16237 (2018).
19. A. Kaushik, A. Vasudev, S. K. Arya, S. K. Pasha, S. Bhansali, Recent advances in cortisol sensing technologies for point-of-care application. *Biosens. Bioelectron.* **53**, 499–512 (2014).
20. S. Yoon, J. K. Sim, Y.-H. Cho, A flexible and wearable human stress monitoring patch. *Sci. Rep.* **6**, 23468 (2016).
21. O. Parlak, A. İncel, L. Uzun, A. P. F. Turner, A. Tiwari, Structuring Au nanoparticles on two-dimensional MoS_2 nanosheets for electrochemical glucose biosensors. *Biosens. Bioelectron.* **89**, 545–550 (2017).
22. A. O. Osikoya, O. Parlak, N. A. Murugan, E. D. Dikio, H. Moloto, L. Uzun, A. P. F. Turner, A. Tiwari, Acetylene-sourced CVD-synthesised catalytically active graphene for electrochemical biosensing. *Biosens. Bioelectron.* **89**, 496–504 (2017).
23. C. B. Nielsen, A. Giovannitti, D.-T. Sbircea, E. Bandiello, M. R. Niazi, D. A. Hanifi, M. Sessolo, A. Amassian, G. G. Malliaras, J. Rivnay, I. McCulloch, Molecular design of semiconducting polymers for high-performance organic electrochemical transistors. *J. Am. Chem. Soc.* **138**, 10252–10259 (2016).
24. G. C. Faria, D. T. Duong, A. Salleo, C. A. Polyzoidis, S. Logothetidis, J. Rivnay, R. Owens, G. G. Malliaras, Organic electrochemical transistors as impedance biosensors. *MRS Commun.* **4**, 189–194 (2014).
25. G. C. Faria, D. T. Duong, A. Salleo, On the transient response of organic electrochemical transistors. *Org. Electron.* **45**, 215–221 (2017).
26. J. Rivnay, R. M. Owens, G. G. Malliaras, The rise of organic bioelectronics. *Chem. Mater.* **26**, 679–685 (2014).
27. P. Leleux, J. Rivnay, T. Lonjaret, J. M. Badier, C. Bénar, T. Hervé, P. Chauvel, G. G. Malliaras, Organic electrochemical transistors for clinical applications. *Adv. Healthc. Mater.* **4**, 142–147 (2015).
28. M. Sessolo, J. Rivnay, E. Bandiello, G. G. Malliaras, H. J. Bolink, Ion-selective organic electrochemical transistors. *Adv. Mater.* **26**, 4803–4807 (2014).
29. S. A. Tria, M. Ramuz, M. Huerta, P. Leleux, J. Rivnay, L. H. Jimison, A. Hama, G. G. Malliaras, R. M. Owens, Dynamic monitoring of *Salmonella typhimurium* infection of polarized epithelia using organic transistors. *Adv. Healthc. Mater.* **3**, 1053–1060 (2014).
30. S. Löffler, B. Libberton, A. Richter-Dahlfors, Organic bioelectronics in infection. *J. Mater. Chem. B* **3**, 4979–4992 (2015).
31. A.-M. Pappa, O. Parlak, G. Scheiblin, P. Mailley, A. Salleo, R. M. Owens, Organic electronics for point-of-care metabolite monitoring. *Trends Biotechnol.* **1**, 45–59 (2018).
32. K. Haupt, K. Mosbach, Molecularly imprinted polymers in chemical and biological sensing. *Biochem. Soc. Trans.* **27**, 344–350 (1999).
33. K. Haupt, Peer reviewed: Molecularly imprinted polymers: The next generation. *Anal. Chem.* **75**, 376 A–383 A (2003).
34. L. Ye, K. Haupt, Molecularly imprinted polymers as antibody and receptor mimics for assays, sensors and drug discovery. *Anal. Bioanal. Chem.* **378**, 1887–1897 (2004).
35. S. Beyazit, B. Tse Sum Bui, K. Haupt, C. Gonzato, Molecularly imprinted polymer nanomaterials and nanocomposites by controlled/living radical polymerization. *Prog. Polym. Sci.* **62**, 1–21 (2016).
36. O. Ramström, L. Ye, K. Mosbach, Artificial antibodies to corticosteroids prepared by molecular imprinting. *Chem. Biol.* **3**, 471–477 (1996).
37. M. Peeters, F. J. Troost, B. van Grinsven, F. Horemans, J. Alenus, M. S. Murib, D. Keszthelyi, A. Ethirajan, R. Thoelen, T. J. Cleij, P. Wagner, MIP-based biomimetic sensor for the electronic detection of serotonin in human blood plasma. *Sens. Actuators B Chem.* **171–172**, 602–610 (2012).
38. D.-H. Kim, J. A. Rogers, Stretchable electronics: Materials strategies and devices. *Adv. Mater.* **20**, 4887–4892 (2008).
39. C. Liang, H. Peng, X. Bao, L. Nie, S. Yao, Study of a molecular imprinting polymer coated BAW bio-mimic sensor and its application to the determination of caffeine in human serum and urine. *Analyst* **124**, 1781–1785 (1999).
40. K. Haupt, K. Mosbach, Molecularly imprinted polymers and their use in biomimetic sensors. *Chem. Rev.* **100**, 2495–2504 (2000).

Acknowledgments: We thank S. Beyazit, A. Sekretaryova, and D. Hanifi for discussions and help. **Funding:** Part of this work was performed at the Stanford Nano Shared Facilities, supported by the NSF under award ECCS-1542152. O.P. acknowledges support from the Knut and Alice Wallenberg Foundation (KAW 2014.0387) for postdoctoral research at Stanford University and the France-Stanford fellowship for travel support. S.T.K. was supported by the Stanford Graduate Fellowship Fund. **Author contributions:** O.P. and A.S. conceived and designed the research. O.P., S.T.K., A.M., and V.F.C. designed and performed the experiments. O.P., S.T.K., and A.S. analyzed the data and wrote the manuscript. **Competing interests:** The authors declare that they have no competing interests. **Data and materials availability:** All data needed to evaluate the conclusions in the paper are present in the paper and/or the Supplementary Materials. Additional data related to this paper may be requested from the authors.

Submitted 23 October 2017
Accepted 4 June 2018
Published 20 July 2018
10.1126/sciadv.aar2904

Citation: O. Parlak, S. T. Keene, A. Marais, V. F. Curto, A. Salleo, Molecularly selective nanoporous membrane-based wearable organic electrochemical device for noninvasive cortisol sensing. *Sci. Adv.* **4**, eaar2904 (2018).